

THE DIRECT PROJECT: CATALOGS OF STELLAR OBJECTS IN NEARBY GALAXIES. I. THE CENTRAL PART OF M33¹

L.M. MACRI, K.Z. STANEK², D.D. SASSELOV³ & M. KROCKENBERGER
 Harvard-Smithsonian Center for Astrophysics, 60 Garden St., Cambridge MA 02138, USA
 lmacri, kstanek, sasselov, krocken@cfa.harvard.edu

&

J. KALUZYNY
 N. Copernicus Astronomical Center, Bartycka 18, PL-00-716 Warszawa, Poland
 jka@camk.edu.pl

ABSTRACT

The DIRECT project aims to determine direct distances to two important galaxies in the cosmological distance ladder – M31 and M33 – using detached eclipsing binaries (DEBs) and Cepheids. The search for these variables requires time-series photometry of large areas of the target galaxies and yields magnitudes and positions for tens of thousands of stellar objects, which may be of use to the astronomical community at large.

During the first phase of the project, between September 1996 and October 1997, we were awarded 95 nights on the F. L. Whipple Observatory 1.2 m telescope and 36 nights on the Michigan-Dartmouth-MIT 1.3 m telescope to search for DEBs and Cepheids in the M31 and M33 galaxies. This paper, the first in our series of stellar catalogs, lists the positions, three-color photometry, and variability indices of 57,581 stars with $14.4 < V < 23.6$ in the central part of M33. The catalog is available from our FTP site.

Subject headings: galaxies: individual (M33) — galaxies: stellar content

1. INTRODUCTION

The DIRECT project (Kaluzny et al. 1998; Stanek et al. 1998) started in 1996 with the long-term goal of obtaining distances to two important galaxies in the cosmological distance ladder – M31 and M33 – using detached eclipsing binaries (DEBs) and Cepheids. These two nearby galaxies are the stepping stones in most of the current effort to understand the evolving universe at large scales. Not only are they essential to the calibration of the extragalactic distance scale, but they also constrain population synthesis models for early galaxy formation and evolution. However, accurate distances are essential to make these calibrations free from large systematic uncertainties.

The search for detached eclipsing binaries and Cepheids in our target fields requires the detection of a large number of stellar objects in our CCD frames and the repeated measurement of their fluxes over a relatively large time baseline, usually of the order of 1-2 years. Since the goal of the project is not simply the detection of these variables but the determination of accurate distances to the target galaxies, we must also undertake a rigorous absolute calibration of our photometry. The resulting catalogs of objects contain tens of thousands of objects, out of which we only select a few hundreds for distance-scale work. However, the astronomical community at large may benefit from the existence of an accurate, well-calibrated list of objects in these nearby, often-studied galaxies. This is our rationale for the publication of these series of catalog papers.

Messier 33 (NGC 598) is one of the main components of the Local Group of galaxies. It is classified as a SA(s)cd

galaxy in the Third Reference Catalog of Galaxies de Vaucouleurs et al. (1991) and as a Sc(s)II-III in the Revised Shapley-Ames Catalog Sandage & Tammann (1981). It is located at a R.A. of $1^{\text{h}}34^{\text{m}}$ and a Declination of $30^{\circ}40^{\text{m}}$ (J2000.0), and it has major and minor B_{25} isophotal diameters of $71'$ and $42'$, respectively. It has been extensively studied, appearing in more than 1000 publications. One of first was that of Hubble (1926), who stated in the abstract of his paper that "... [i]ts great angular diameter and high degree of resolution, suggesting that it is one of the nearest objects of its kind, offer exceptional opportunities for detailed investigation."

The present work will describe the details of the observations (§2), the reduction and absolute calibration of the data (§3), the creation of the stellar catalog (§4) and the results of our consistency checks (§5) for three CCD fields in the central part of M33. The analysis of the variable stars located in these fields will be analyzed in two upcoming papers by Macri et al. (2001) and Stanek et al. (2001).

2. OBSERVATIONS

Our observations of the central region of M33 were primarily carried out at the Fred L. Whipple Observatory (hereafter FLWO) 1.2-m telescope. We used "AndyCam" (Szentgyorgyi et al. 2000), a thinned, back-illuminated, AR-coated Loral 2048² pixel CCD camera with a plate scale of $0.317''/\text{pixel}$, or an effective field of view of $10''.8$. The filters used during our program were standard Johnson B and V and Cousins I . Additional I -band data were collected at the Michigan-Dartmouth-MIT Observatory 1.3-m McGraw-Hill telescope. We used "Wilbur" (Met-

¹ Based on observations collected at the Fred L. Whipple Observatory 1.2-m telescope and at the Michigan-Dartmouth-MIT 1.3-m telescope.

² Hubble Fellow

³ Alfred P. Sloan Foundation Fellow

zger et al. 1993), a thick, front-illuminated Loral 2048² pixel CCD camera. The plate scale and field of view were almost identical to that of “AndyCam.”

We observed three fields located north, south and southwest of the center of M33, which we labeled M33A, B and C. The J2000.0 center coordinates of the fields are: M33A, R.A. = 01^h34^m05.1^s, Dec. = 30°43′43″; M33B, R.A. = 01^h33^m55.9^s, Dec. = 30°34′04″; M33C, R.A. = 01^h33^m16.0^s, Dec. = 30°35′15″. Figure 1 shows the boundaries of these fields overlaid on a digitized image of the galaxy from the POSS-I survey⁴, while Figure 2 shows a mosaic of the survey fields, created with our CCD data. At FLWO, we obtained *V* and *I* data on 42 nights and *B* data on 13 nights. At MDM, we obtained *I* data on 10 nights. Exposure times were 1200s in *B*, 900s in *V* and 600s in *I*. Fields were observed repeatedly on each night in *V* and *I*, so the actual number of exposures per field in those filters is around 110 and 60, respectively. Standard star fields from Landolt (1992) were observed on one photometric night. Table 1 presents a log of our observations.

3. DATA REDUCTION AND CALIBRATION

3.1. PSF photometry

Paper I of the DIRECT variable star series (Kaluzny et al. 1998) contains a detailed description of the data reduction and PSF photometry. Only a brief summary of these procedures is presented here. The CCD frames were processed using standard CCDPROC routines under IRAF⁵. Photometry was obtained using the DAOPHOT and ALLSTAR programs (Stetson 1987, 1992), using a Tcl/Tk-based automated reduction pipeline.

Point-spread functions (PSFs) were calculated from bright and isolated stars present in each frame, following an iterative process. Figure 3 shows a histogram of the seeing for the three filters; median FWHM values were 1.5″ for *I* and 1.8″ for *B* and *V*. After running DAOPHOT and ALLSTAR on all frames, we selected an image of particularly good quality (in terms of seeing and depth) as a “template” frame. ALLSTAR was run again in “fixed-position” mode on all other images, using the transformed object list from the template frame as input. The resulting photometry lists were transformed back into the coordinate and instrumental magnitude system of the template image. The latter was accomplished by computing a local magnitude offset for each star, using high SNR stars ($\sigma < 0.03$ mag) located within a radius of 350 pixels. In cases where few stars met these conditions, the search radius was increased to 750 pixels, or a global median offset was used as a last resort. The magnitude offset between each frame and the template image was recorded in a log file for future use (see below). The typical uncertainty in this offset was 0.02 mag.

Thus, for each field and filter combination, the output of our automated reduction pipeline consisted of one ALLSTAR file for each frame, with positions and PSF magnitudes in the coordinate and photometric systems of its template frame. The ALLSTAR files pertaining to a

particular field and filter combination were matched and merged, to arrive at nine final photometry databases (3 fields \times 3 filters).

The instrumental PSF magnitudes present in the databases had to be transformed into the standard system. This procedure can be separated into three steps: i) transform PSF magnitudes in the instrumental system of the template frame to PSF magnitudes in the instrumental system of the photometric frame; ii) transform PSF magnitudes in the instrumental system of the photometric frame to aperture magnitudes in the instrumental system of the photometric frame; iii) transform the instrumental system of the photometric frame to the standard system. These steps are described in detail below.

3.2. Aperture corrections

The first step of the photometric calibration process was the transformation of the PSF magnitudes of the photometry database from the magnitude scale of the template frame to the magnitude scale of another frame, taken under photometric conditions (hereafter referred to as the “photometric frame”). This was easily achieved by applying a magnitude offset of equal size and opposite sign to the one which had already been determined (as part of our automated pipeline) to exist between the template frame and the photometric frame.

The second step of the process was the transformation of PSF magnitudes into aperture magnitudes, through the determination of aperture correction coefficients. Given the crowded nature of our fields, their rapidly-varying sky backgrounds, and the relatively poor seeing of our photometric night, a thorough approach was required. We chose one frame for each field and filter from the photometric night, and used the master star lists and the PSFs derived by our automated pipeline to remove all objects present in these images, with the exception of bright, isolated stars. Aperture photometry was carried out on these star-subtracted frames at a variety of radii (ranging from 10 to 20 pixels, or 3 to 6″). The local sky was characterized using an annulus extending from 30 to 40 pixels.

The aperture photometry measurements of all bright stars in a particular frame were examined simultaneously by visually inspecting their curves of growth (i.e., plots of aperture magnitude versus radius). Objects with unusual growth curves were discarded. The aperture photometry measurements of the remaining bright stars (hereafter, “input stars”) were analyzed using DAOGROW (Stetson 1990). This program performs an analytical fit to the growth curves of all input stars in all frames, and the resulting function is used to determine a mean growth curve for each frame. DAOGROW then uses the best combination of aperture photometry and growth curve for each input star to calculate its aperture magnitude at the outermost radius (in our case, 20 pixels). Lastly, the PSF and aperture magnitudes of all input stars in each frame are used to derive a mean value of the aperture correction, which is applied to all objects. The aperture correction co-

⁴ The Digitized Sky Surveys were produced at the Space Telescope Science Institute under U.S. Government grant NAGW-2166. The National Geographic Society – Palomar Observatory Sky Atlas (POSS-I) was made by the California Institute of Technology with grants from the National Geographic Society.

⁵ IRAF is distributed by the National Optical Astronomy Observatories, which are operated by the Associations of Universities for Research in Astronomy, Inc., under cooperative agreement with the NSF.

efficients derived using this procedure ranged from -0.10 to $+0.24$ mag, with typical uncertainties of 0.03 mag.

3.3. Photometric solutions

Once the instrumental PSF magnitudes in each of the nine databases were converted to instrumental aperture magnitudes, the last step required to transform them into standard magnitudes was the derivation of photometric zeropoints. On 1997 October 9, a photometric night of average seeing quality for our program (I: $1.8''$; B and V: $2.0''$), we observed six fields from Landolt (1992), containing a total of forty-three standard stars, at airmasses ranging from 1.12 to 2.12. We performed photometry on the standard stars using DAOPHOT with the same settings used for the program stars, namely an aperture radius of 20 pixels and a sky annulus extending from 30 to 40 pixels. We used the IRAF PHOTCAL routines to solve for a photometric solution of the form

$$M_{std,i} = m_{obs,i} + \chi_i - k'_i X + \xi_{ij}(M_{std,i} - M_{std,j}) \quad (1)$$

where $M_{std,i}$ and $M_{std,j}$ are the magnitudes of a star in the standard system in the i and J filters, while $m_{obs,i}$ is the instrumental magnitudes of the same star in the i filter. χ_i is the magnitude zeropoint at $X = 0$, k'_i is the airmass coefficient for the i filter, and ξ_{ij} is the color term. The V-band solution was calculated using both B-V and V-I for the color term; the latter one was used by default in the calibration process, unless only B and V data were available for a particular object. The B-band solution was calculated using B-V for the color term, while the I-band solution was calculated using V-I for the color term. The values and uncertainties of the coefficients of each term are presented in Table 2; based on those numbers, we estimate a total uncertainty of ± 0.02 mag in our solutions.

Based on the uncertainties associated with PSF magnitude offsets (± 0.02 mag, §3.1), aperture correction coefficients (± 0.03 mag, §3.2) and photometric solutions (± 0.02 mag, previous paragraph), we estimate a total random uncertainty in our photometric zeropoints of ± 0.04 mag.

4. THE STAR CATALOG

Once the photometric calibrations were applied, we merged the *BVI* databases of each field into a single catalogs. Objects were matched from the master B, V and I star lists of each field and were kept only if they had been detected in the V band and in either of the B or I bands. Next, we transformed the object coordinates into the FK5 system using stars from the USNO-A2.0 catalog (Monet et al. 1998). We solved for a cubic-order transformation using software developed by Mink (1999). The solutions used 30-70 stars and had *rms* values of $0.4''$.

Lastly, the catalogs of the three fields were merged into a single, master catalog. There was –by design– significant overlap between fields A and B as well as between fields C and B; objects in these regions were matched to test the internal consistency of our astrometric and photometric calibrations (see §5). To avoid duplication of these objects, we only kept the entry from field B.

As described in Kaluzny et al. (1998), the magnitude uncertainties reported by DAOPHOT/ALLSTAR are under-estimated for bright stars and over-estimated

for faint ones. The errors were re-scaled following the precepts established in that paper. Lastly, we calculated mean BVI magnitudes and V-band J_S variability indices (Stetson 1996). The catalog is presented in Table 3; it lists IDs, celestial coordinates, mean B, V and I magnitudes and uncertainties, and J_S indices for 57,581 stars present in our fields. The catalog can also be retrieved from the DIRECT FTP site at <http://cfa-www.harvard.edu/~kstanek/DIRECT>.

Figure 4 shows the differential luminosity function of the objects in our catalog. The turnovers in these luminosity functions indicate incompleteness below ~ 22 mag for B and V, and ~ 20 mag for I. Figure 5 shows color-magnitude diagrams of our catalog stars. A faint plume of foreground stars from our own Galaxy can be seen in the region $0.4 < B - V < 1.2$, $V < 20$. The feature is substantially diminished relative to the one seen in the CMD of M31 in Kaluzny et al. (1998) due to the difference in galactic latitude between these two objects ($l \sim -22^\circ$ for M31 and $l \sim -31^\circ$ for M33).

We flagged objects as candidate variables if they met two requirements: a J_S index larger than 0.75, and a V-band magnitude uncertainty larger than 0.04 mag. The second criterion was introduced to remove bright stars with small variability from our sample of candidate variables (in this data set, it removed 107 stars with $V < 19.5$ mag). Our final sample of candidate variables consists of 1,298 stars. The panels of Figure 6 show some global properties of the variable stars present in our catalog.

5. TEST OF PHOTOMETRIC AND ASTROMETRIC CALIBRATIONS

We used ~ 5000 objects present in the overlap regions between the survey fields to check our astrometric and photometric calibration procedures. We compared the celestial coordinates of these objects and found small offsets between fields of the order of $0''.4 - 0''.7$, which are consistent with the *rms* residuals of the astrometric solutions.

We performed an internal test of our photometric calibration by comparing the mean B, V and I magnitudes of bright stars present in the overlap regions. We imposed magnitude cuts of 19.5, 19.5 and 19.0 mag in B, V, and I, respectively, which restricted the number of matches to about 200, 300 and 400, respectively. On average, the offsets were < 0.01 mag. This indicates that PSF variations across the field were properly taken into account by DAOPHOT and our pipeline, and that the aperture corrections were properly determined. Table 4 lists the values of the offsets and their standard deviations; Figure 7 shows plots of these comparisons.

We performed two external tests of our photometric calibration. In the first test, we matched about 200 objects in common between our Field C and Field 4 of Wilson, Freedman & Madore (1990). We compared the mean B, V and I magnitudes of stars brighter than 20.0 mag in each of the filters (about 25 stars/filter) and found offsets of the order of -0.03 mag (brighter DIRECT magnitudes). In the second external test of our photometric calibration, we matched about 4000 objects in common between our Field A and one of the fields of Bersier et al. (2001). We compared the mean B and V magnitudes of stars brighter

than 18.5 mag (about 35 stars/filter) and again found offsets of the order of -0.03 mag (brighter DIRECT magnitudes). Table 4 lists the results of these comparisons, which are also plotted on Figures 8 and 9.

6. ARTIFICIAL STAR TESTS

The differences between our photometry and the Wilson, Freedman & Madore (1990) and Bersier *et al.* (2001) photometry are small but consistent. Furthermore, both groups used larger telescopes (CFHT and WIYN, respectively) under significantly better seeing conditions than us. Therefore, we decided to undertake artificial star tests to quantify the level of photometric bias that could arise due to the poorer spatial resolution of our images.

We used DAOPHOT to inject 2,500 artificial stars into the nine master frames, using the PSFs previously derived by our automated reduction pipeline and taking into account photon noise and other detector characteristics. We analyzed the frames using the same procedures as in the automated pipeline. The results were quite similar for the three frames pertaining to each band, and thus the data files were merged to improve the statistics. Our results are presented in Table 5 and in Figure 10.

Bright stars ($15 < m < 18$) are affected by crowding at the 0.01 – 0.04 mag level. The bias becomes stronger for fainter objects ($m > 18$), reaching 0.05 – 0.08 mag. At a given magnitude, the bias increases from B to V to I. In all cases, the offset induced by crowding is in the same direction as the offset found between our data and other catalogs.

7. SUMMARY

We have observed three fields in the central part of M33 at the Fred L. Whipple Observatory 1.2-m and the Michigan-Dartmouth-MIT Observatory 1.3-m telescopes. We have performed PSF photometry of objects in these fields, calibrated in the standard system with a zeropoint accuracy of ± 0.04 mag.

We have compiled a catalog of positions, B, V and I magnitudes, and V-band variability indices for 57,581 stars with $14.4 < V < 23.6$. The catalog is available from our FTP site.

The analysis of the variable star content of these fields will be presented in two upcoming papers by Macri *et al.* (2001) and Stanek *et al.* (2001).

We would like to thank the telescope allocation committees of the FLWO and MDM Observatories for the generous amounts of telescope time devoted to this project. We would also like to thank Peter Stetson, for his photometry software; Doug Mink, for help with the astrometry; and David Bersier, for providing us his photometry in advance of publication. LMM would like to thank John Huchra for his support and comments. KZS was supported by a Hubble Fellowship grant HF-01124.01-99A from the Space Telescope Science Institute, which is operated by the Association of Universities for Research in Astronomy, Inc., under NASA contract NAS5-26555. DDS acknowledges support from the Alfred P. Sloan Foundation and from NSF grant No. AST-9970812. JK was supported by KBN grant 2P03D003.17

REFERENCES

- Bersier, D., Wood, P.R., Mould, J.R., Hoessel, J.G., Tanvir, N.R. & Hughes, S.M.G. 2001, in preparation
- de Vaucouleurs, G., de Vaucouleurs, A., Corwin Jr., H., Buta, R., Paturel, G. & Fouqué, P. 1991, *Third Reference Catalogue of Bright Galaxies* (Berlin: Springer-Verlag)
- Hubble, E.P. 1926, *ApJ*, 63, 236
- Kaluzny, J., Stanek, K.Z., Krockenberger, M., Sasselov, D.D., Tonry, J.L. & Mateo, M. 1998, *AJ*, 115, 1016
- Landolt, A.U. 1992, *AJ*, 104, 340
- Macri, L.M., Stanek, K.Z., Krockenberger, M., Sasselov, D.D. & Kaluzny, J. 2001, *AJ*, in preparation
- Metzger, M.R., Tonry, J.L. & Luppino, G.A. 1993, in ASP Conf Ser. 52, *Astronomical Data Analysis Software and Systems II*, eds. R.J. Hanisch, R.J.V. Brissenden & J. Barnes (San Francisco: ASP), p. 300
- Mink, D.J. 1999, in ASP Conf. Ser. 172, *Astronomical Data Analysis Software and Systems VIII*, eds. G. Hunt & H.E. Payne (San Francisco: ASP), p. 249
- Monet, D., *et al.* 1998, USNO-A2.0, (Washington: U.S. Naval Observatory)
- Sandage, A. and Tammann, G. 1981, *Revised Shapley-Ames Catalog of Bright Galaxies* (Washington: Carnegie)
- Stanek, K.Z., Kaluzny, J., Krockenberger, M., Sasselov, D.D., Tonry, J.L. & Mateo, M. 1998, *AJ*, 115, 1894
- Stanek, K.Z., Macri, L.M., Sasselov, D.D., Krockenberger, M., & Kaluzny, J. 2001, *AJ*, in preparation
- Stetson, P.B. 1987, *PASP*, 99, 191
- Stetson, P.B. 1990, *PASP*, 102, 932
- Stetson, P.B. 1992, in ASP Conf. Ser. 25, *Astronomical Data Analysis Software and Systems I*, eds. D.M. Worrall, C. Bimesderfer & J. Barnes (San Francisco: ASP), p. 297
- Stetson, P.B. 1996, *PASP*, 108, 851
- Szentgyorgyi, A.H., *et al.* 2000, in preparation.
- Wilson, C., Freedman, W.L. & Madore, B.F. 1990, *AJ*, 99, 149

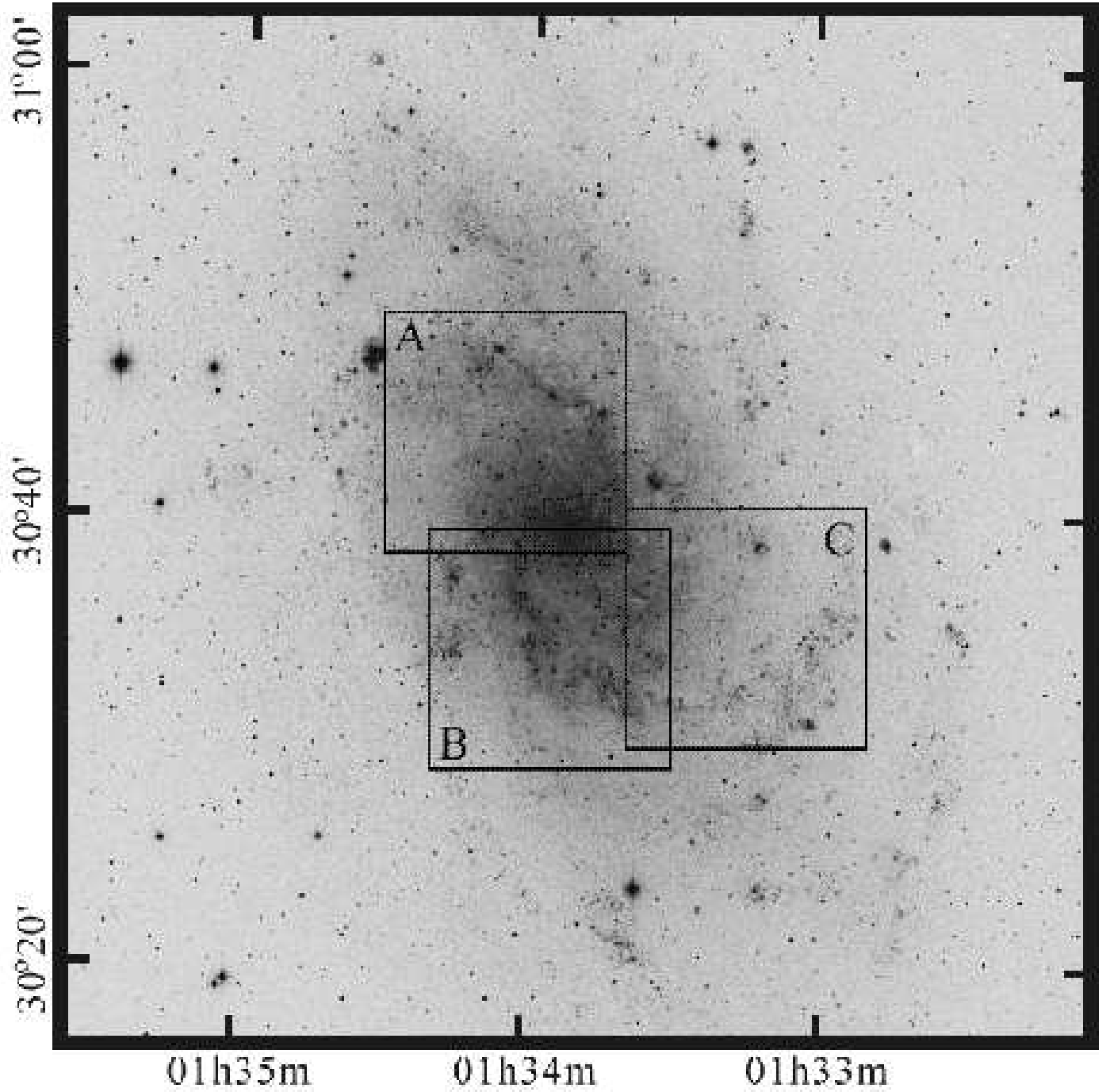


FIG. 1.— Palomar Observatory Sky Survey image of M33, showing the size and location of fields A-C. Each box is approximately $10'8''$ on a side. North is up and East is to the left.

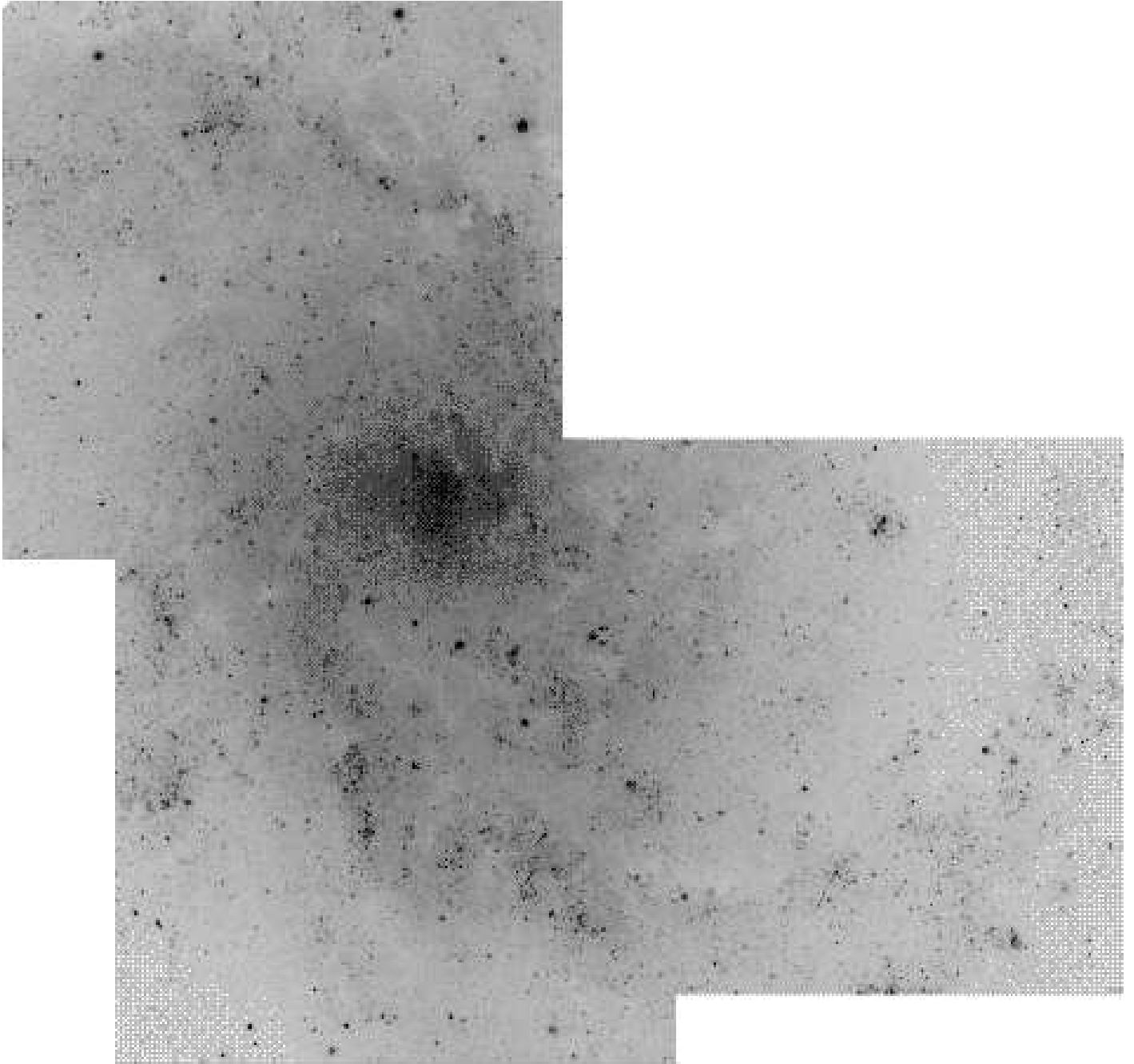


FIG. 2.— Mosaic of the central part of M33, created from CCD images of our fields.

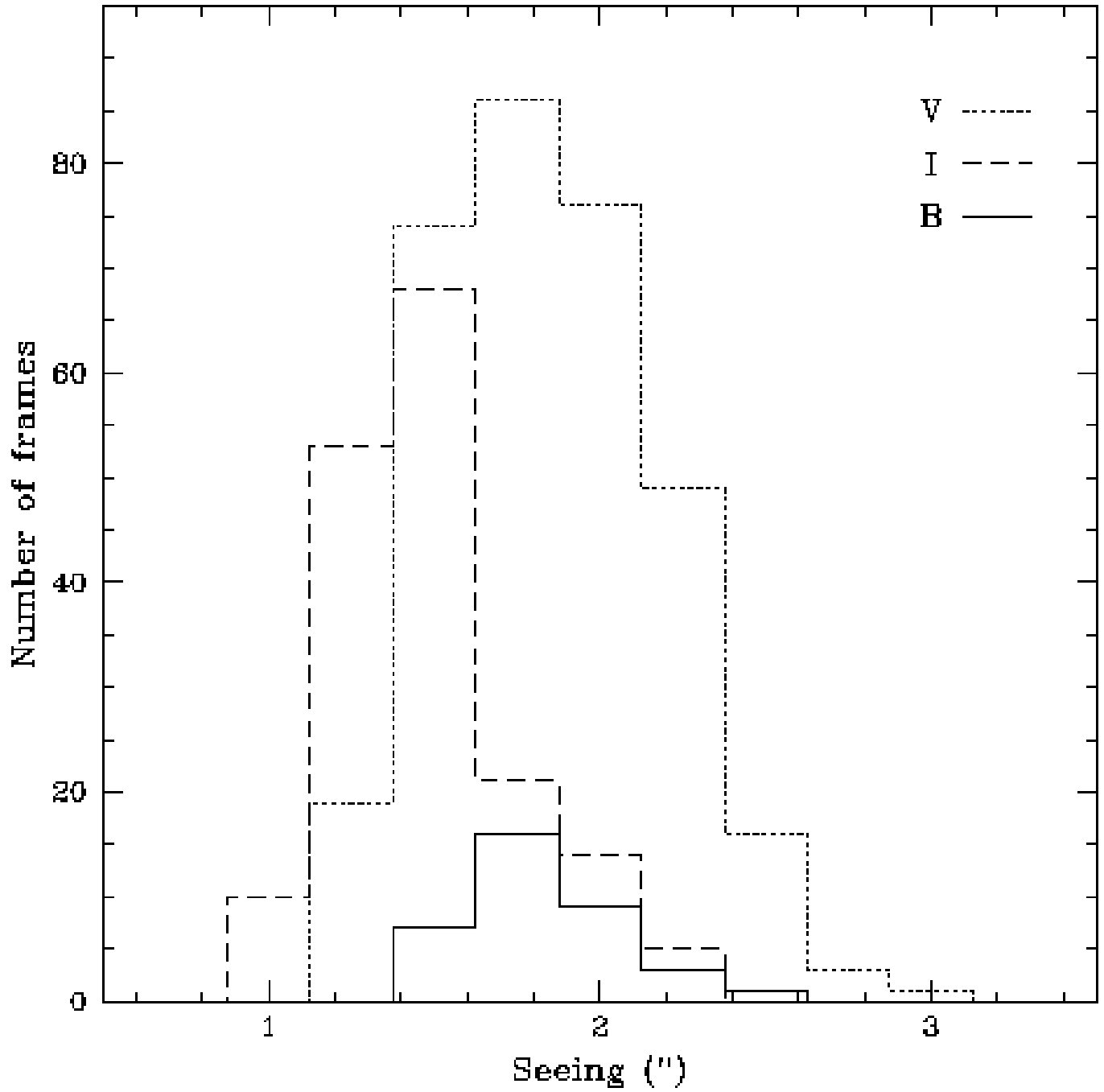


FIG. 3.— Histogram of seeing values for the frames acquired for this project. Solid, dotted and dashed lines represent the B, V and I band histograms, respectively.

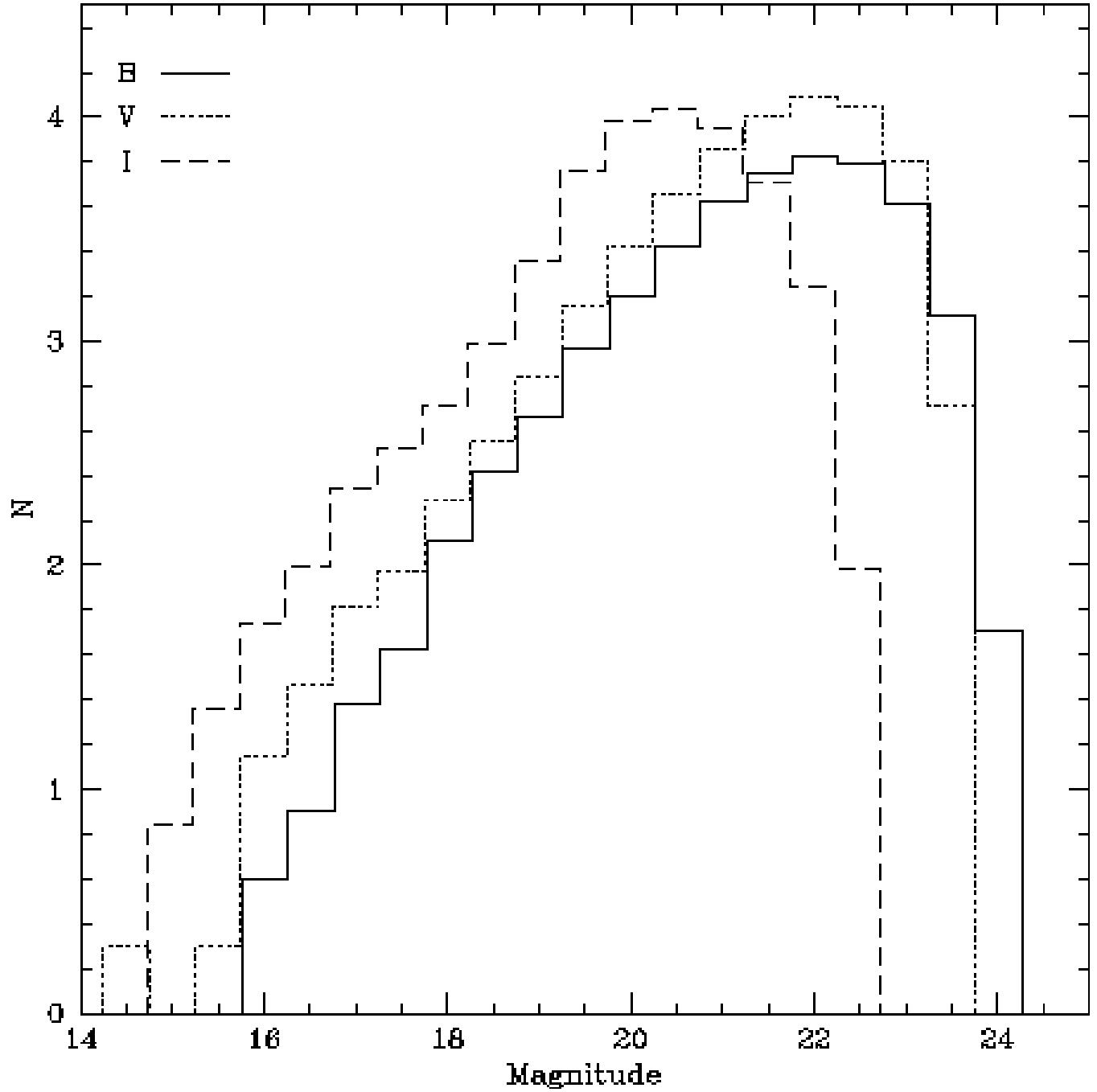


FIG. 4.— Differential luminosity functions for the stars present in our catalog, for the B (solid), V (dashed) and I (dotted) bands. Our completeness limits are ~ 22 mag for B and V and ~ 20 mag for I.

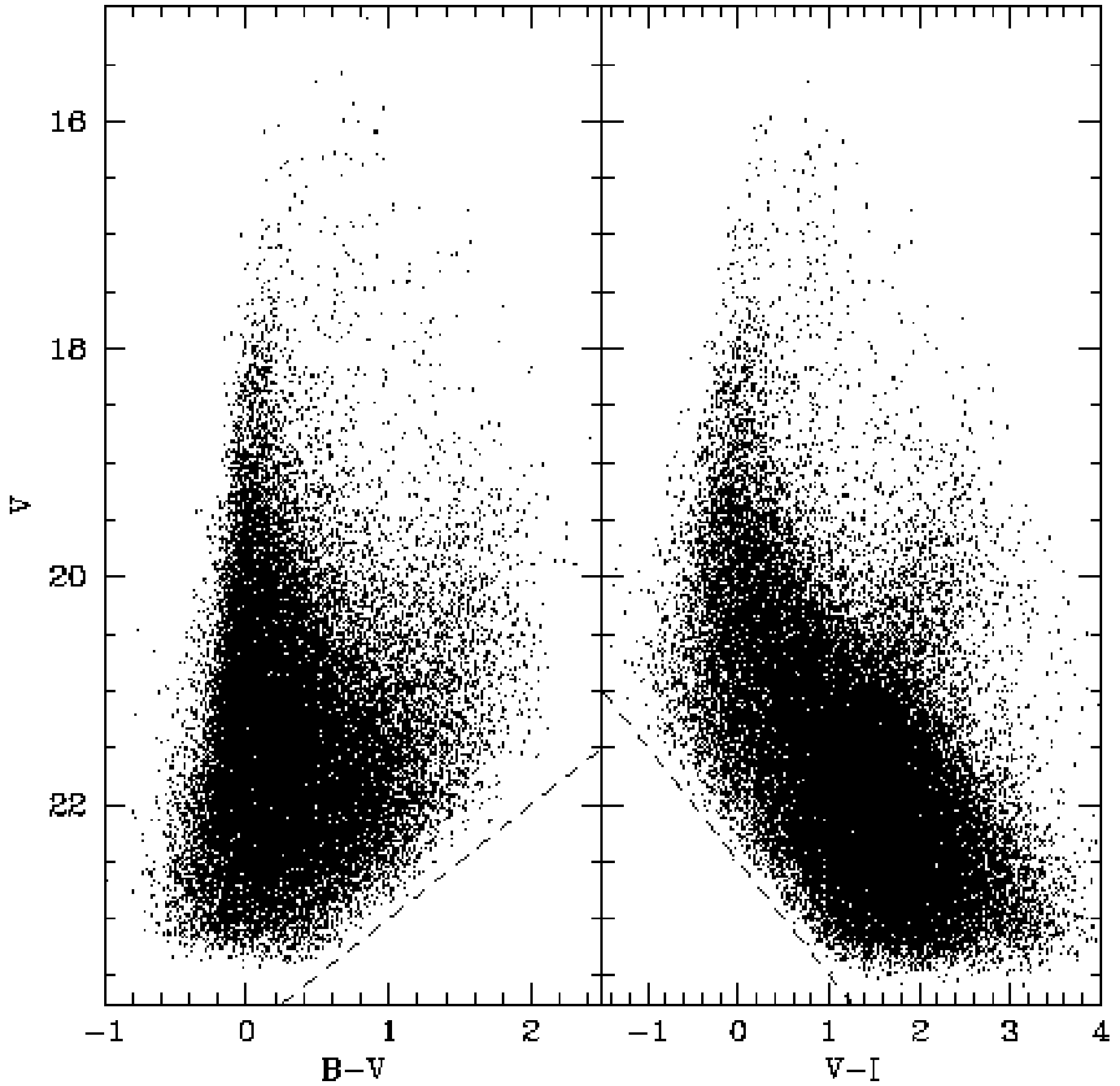


FIG. 5.— Color-magnitude diagrams for the stars present in our catalog. The dashed lines indicate the extent of our data, set by our limiting magnitudes of $B \sim 24$ and $I \sim 22$.

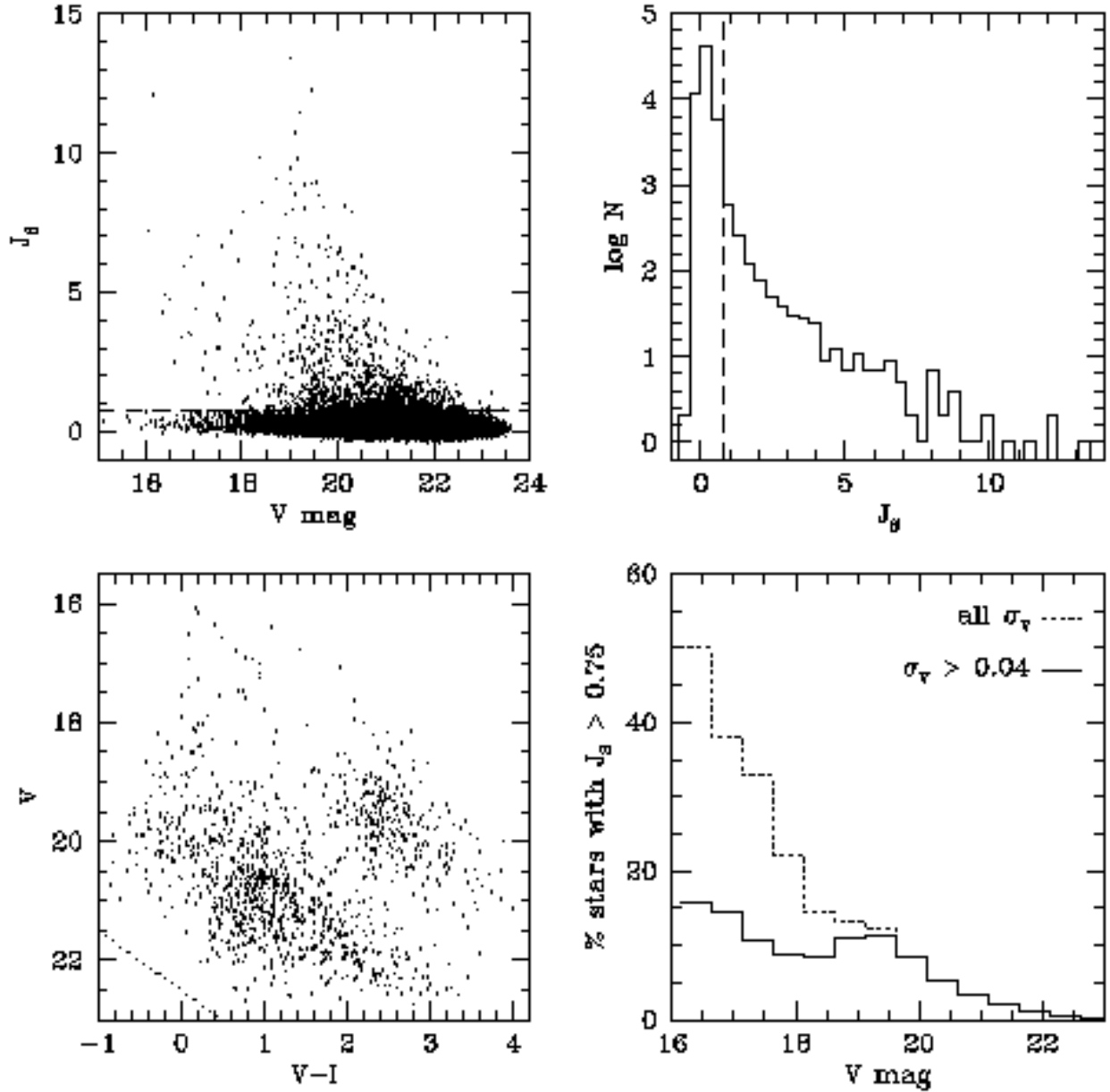


FIG. 6.— Global properties of candidate variables present in our catalog. Top left: Distribution of J_S with V mag. The dashed line indicates our threshold of $J_S = 0.75$. Top right: Number of stars in the catalog as a function of J_S value. The dashed line indicates our threshold of $J_S = 0.75$. Bottom left: Color-magnitude diagram of candidate variables. The dotted line indicates the extent of our data. Bottom right: Effect of imposing a $\sigma_V > 0.04$ mag cut in our definition of variability; a large percentage of bright stars are dropped from the candidate variable sample.

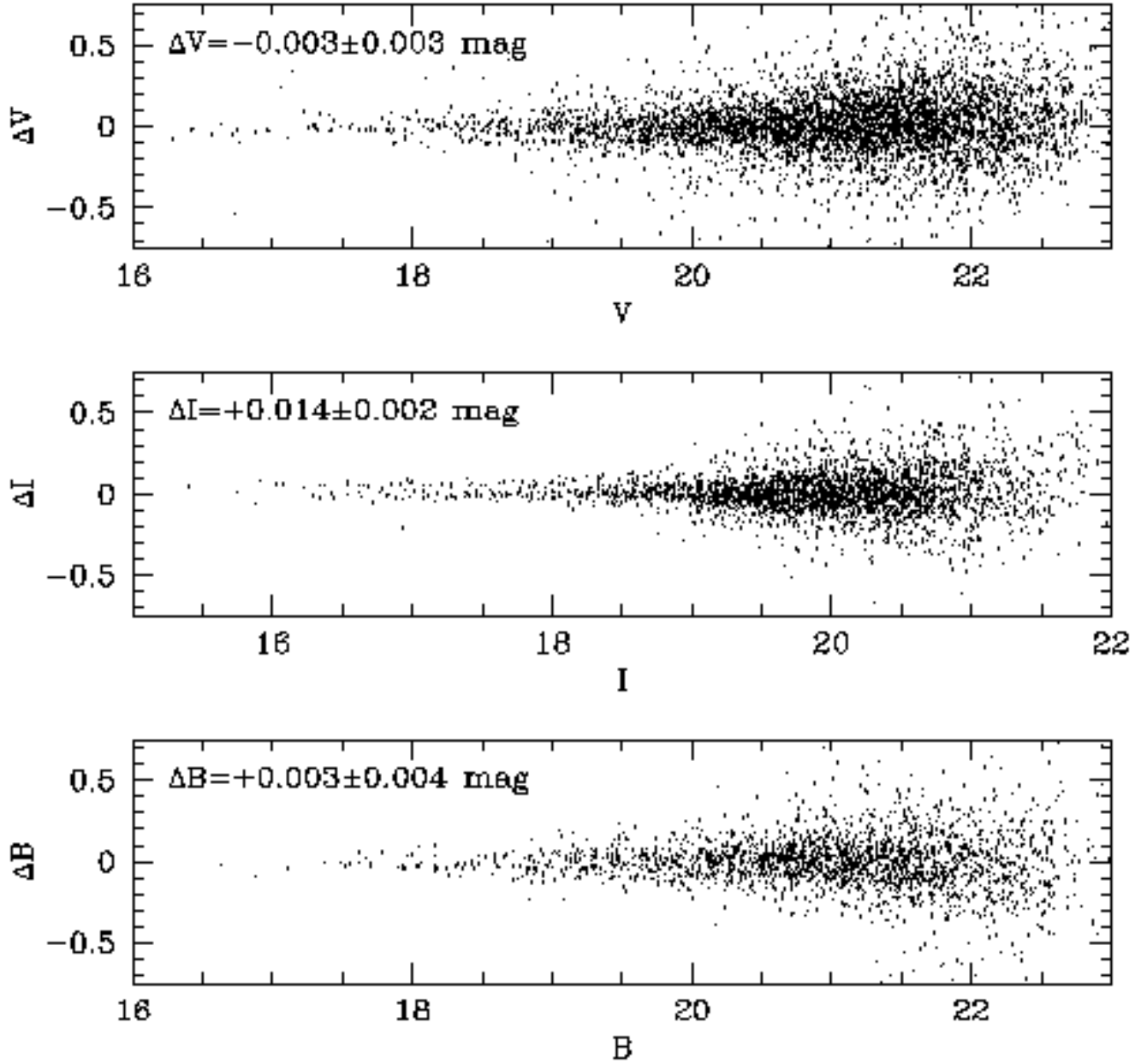


FIG. 7.— Comparison of mean magnitudes for bright stars ($B < 19.5$ mag; $V < 19.5$ mag; $I < 19.0$ mag) located in the overlap regions between fields A-B and C-B. The photometric zeropoints and aperture correction coefficients are determined independently for each field, so these comparisons allow us to check the internal consistency of our reductions. The average values and *r.m.s.* deviations of the offsets are listed in the top-left corner of each panel and in Table 4.

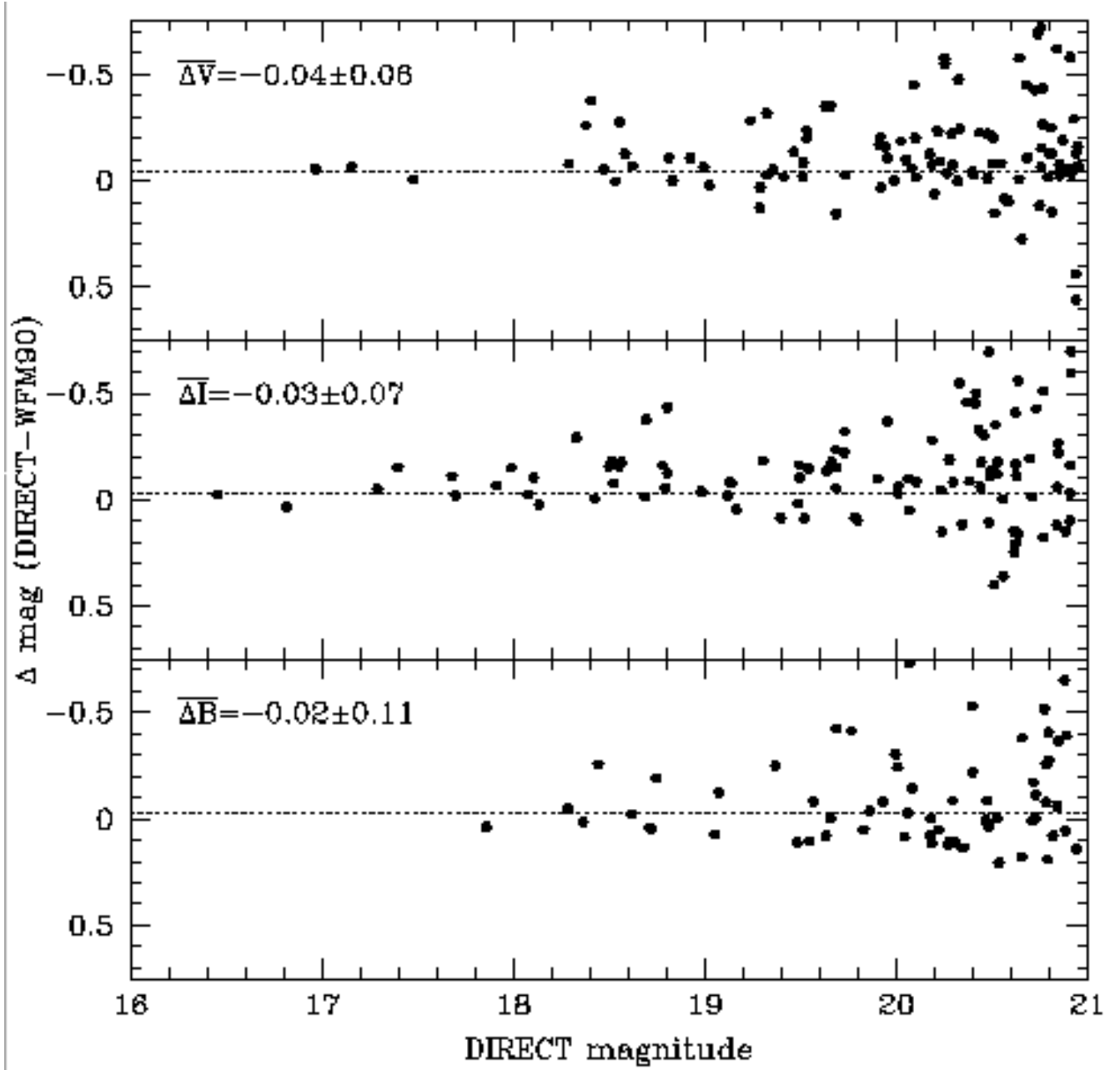


FIG. 8.— Comparison of mean magnitudes for bright stars ($B, V, I < 20$ mag) in common between Field C and Field 4 of Wilson, Freedman & Madore (1990). The average values and *r.m.s.* deviations of the offsets are listed in the top-left corner of each panel and in Table 4.

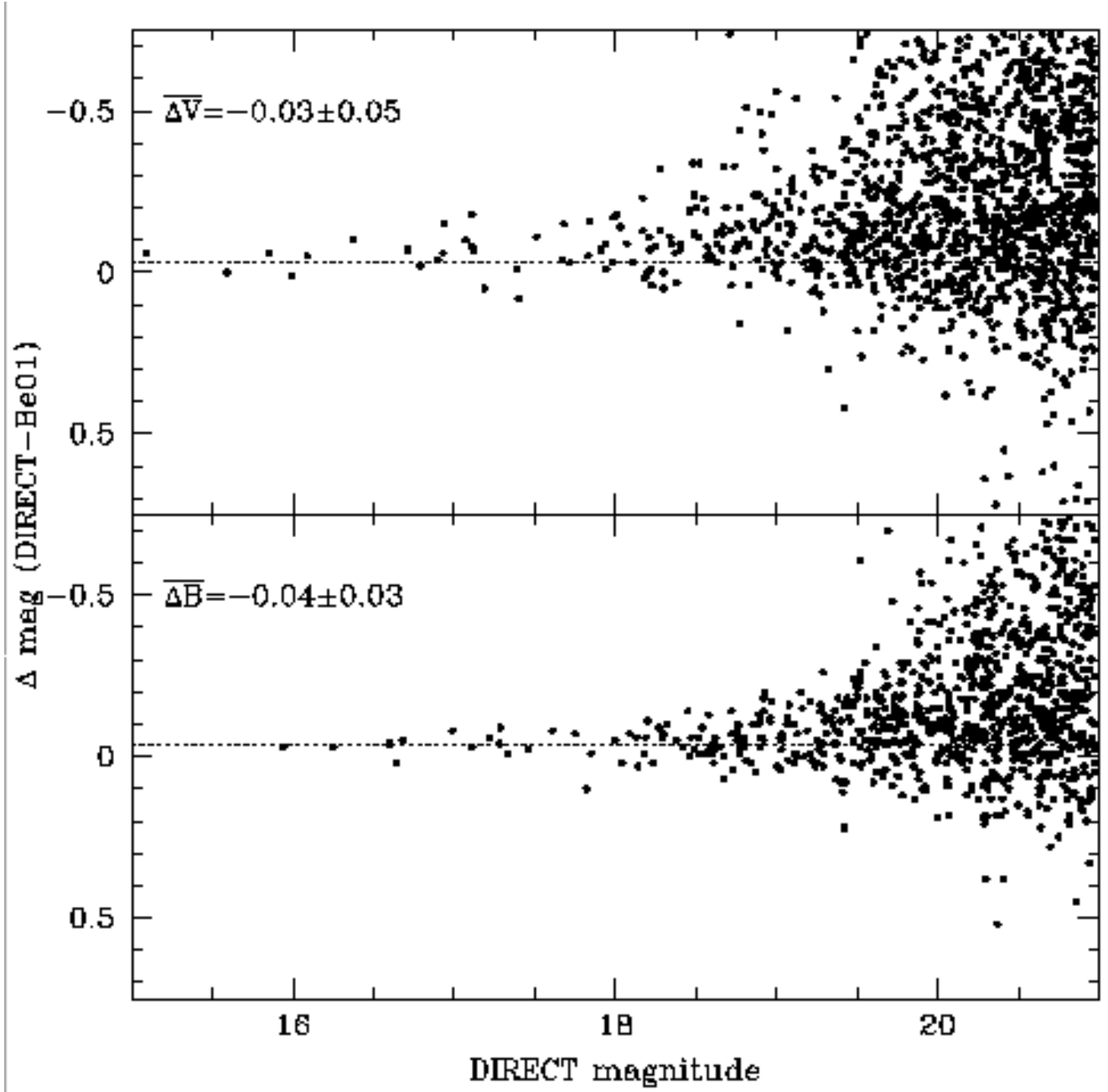


FIG. 9.— Comparison of mean magnitudes for bright stars ($B, V < 18.5$ mag) in common between Field A and one of the fields of Bersier et al. (2001). The average values and *r.m.s.* deviations of the offsets are listed in the top-left corner of each panel and in Table 4.

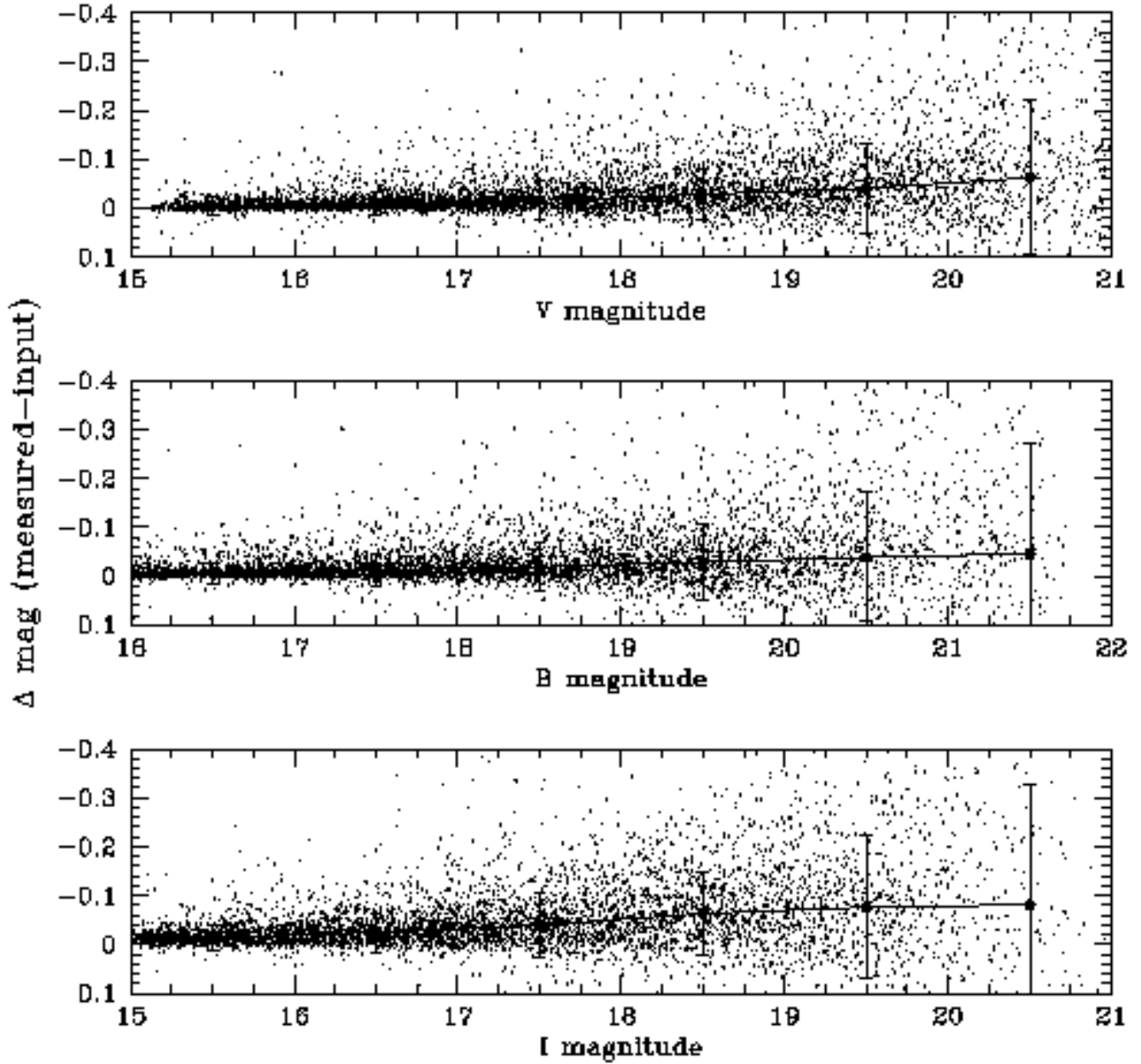


FIG. 10.— Results of the artificial star tests. Individual stars are plotted using small dots, while median values for one-magnitude intervals are indicated with solid circles. They are also listed in Table 5.

TABLE 1
LOG OF OBSERVATIONS

UT Date	MJD	Field	Band	Tel.	Seeing
1996/09/03	329.7615	M33A	I	F	1.40
	329.7786	M33A	I	F	1.24
1996/09/06	332.7220	M33A	V	F	2.18
	332.7504	M33A	V	F	2.25
	332.7735	M33A	V	F	1.77
	332.7803	M33A	V	F	1.84
	332.8479	M33B	B	F	2.03
	332.8697	M33B	V	F	1.82
	332.8814	M33B	V	F	1.37
	332.8932	M33B	V	F	1.43
	332.9114	M33C	V	F	1.39
	332.9182	M33C	V	F	1.57
	332.9434	M33C	V	F	1.82
	332.9612	M33C	I	F	1.28
	332.9669	M33B	I	F	1.36
	332.9753	M33A	I	F	1.28
	332.9873	M33A	V	F	1.34
1996/09/07	333.8863	M33A	V	F	1.68
	333.8930	M33A	V	F	1.70
	333.9047	M33A	I	F	1.07
	333.9130	M33B	I	F	1.22

Continues in electronic form

Note. — Telescope code: F=FLWO; M=MDM.
‡: Photometric night – Standards observed.

TABLE 2
PHOTOMETRIC SOLUTION FOR 1997 OCT 09

Filter	χ	k'	ξ	rms
B (B-V)	-22.953 ± 0.025	0.212 ± 0.017	-0.033 ± 0.011	0.030
V (B-V)	-22.714 ± 0.014	0.123 ± 0.009	0.035 ± 0.006	0.016
V (V-I)	-22.720 ± 0.013	0.127 ± 0.009	0.032 ± 0.005	0.016
I (V-I)	-22.719 ± 0.016	0.064 ± 0.010	-0.051 ± 0.007	0.021

TABLE 3
CATALOG OF STARS IN THE CENTRAL PART OF M33

ID	R.A.	Dec.	V	I	B	σ_V	σ_I	σ_B	J_S
D33 J013251.1+303923.7	01 32 51.11	30 39 23.65	19.97	18.14	...	0.03	0.03	...	0.12
D33 J013251.1+303741.8	01 32 51.13	30 37 41.81	21.61	21.65	...	0.11	0.28	...	0.12
D33 J013251.1+303954.9	01 32 51.14	30 39 54.86	21.72	19.50	...	0.12	0.13	...	0.06
D33 J013251.2+303736.4	01 32 51.17	30 37 36.44	20.20	19.61	...	0.04	0.08	...	0.09
D33 J013251.2+303907.1	01 32 51.20	30 39 07.09	22.87	21.82	...	0.26	0.27	...	-0.02
D33 J013251.2+303648.7	01 32 51.20	30 36 48.67	21.32	21.57	...	0.10	0.17	...	0.04
D33 J013251.2+303959.6	01 32 51.22	30 39 59.58	22.64	21.32	...	0.52	0.28	...	0.64
D33 J013251.2+303607.0	01 32 51.22	30 36 06.95	23.13	20.14	...	0.22	0.15	...	0.04
D33 J013251.2+303944.1	01 32 51.22	30 39 44.10	21.63	...	22.44	0.14	...	0.11	-0.02
D33 J013251.2+303757.4	01 32 51.22	30 37 57.43	22.21	21.01	...	0.18	0.17	...	0.08
D33 J013251.2+303855.7	01 32 51.25	30 38 55.68	22.79	21.24	...	0.30	0.25	...	-0.12
D33 J013251.2+303947.4	01 32 51.25	30 39 47.45	22.91	21.56	...	0.28	0.23	...	0.11
D33 J013251.3+303646.9	01 32 51.25	30 36 46.87	22.00	20.37	...	0.15	0.13	...	-0.09
D33 J013251.3+303936.8	01 32 51.27	30 39 36.79	22.67	21.10	...	0.23	0.19	...	0.08
D33 J013251.3+304013.5	01 32 51.30	30 40 13.51	22.31	22.10	22.35	0.19	0.34	0.09	-0.05
D33 J013251.3+303952.3	01 32 51.30	30 39 52.34	22.64	21.34	...	0.22	0.18	...	0.02
D33 J013251.3+303913.1	01 32 51.31	30 39 13.11	20.88	19.28	21.86	0.06	0.05	0.03	0.14
D33 J013251.3+303802.8	01 32 51.32	30 38 02.76	22.27	20.93	...	0.18	0.19	...	-0.00
D33 J013251.3+303719.3	01 32 51.32	30 37 19.27	22.70	19.79	...	0.23	0.08	...	0.22
D33 J013251.3+303650.6	01 32 51.32	30 36 50.61	22.88	21.59	...	0.29	0.22	...	0.04
D33 J013251.3+303539.1	01 32 51.33	30 35 39.12	21.94	21.27	...	0.24	0.25	...	0.45
D33 J013251.3+303842.9	01 32 51.34	30 38 42.87	22.89	20.45	...	0.28	0.17	...	0.26
D33 J013251.3+303701.1	01 32 51.34	30 37 01.06	22.35	19.72	...	0.18	0.11	...	0.04
D33 J013251.3+303940.1	01 32 51.35	30 39 40.07	23.18	20.55	23.67	0.30	0.11	0.17	0.05
D33 J013251.3+303644.0	01 32 51.35	30 36 43.95	20.57	18.78	...	0.06	0.04	...	-0.04
D33 J013251.3+303823.0	01 32 51.35	30 38 23.03	20.75	21.09	20.79	0.06	0.23	0.02	-0.07
D33 J013251.3+304009.5	01 32 51.35	30 40 09.48	22.86	...	23.20	0.36	...	0.19	0.56
D33 J013251.3+303703.3	01 32 51.35	30 37 03.29	23.24	21.51	...	0.35	0.28	...	0.11
D33 J013251.4+303814.2	01 32 51.35	30 38 14.21	23.15	21.93	23.66	0.35	0.31	0.25	0.10
D33 J013251.4+303726.9	01 32 51.35	30 37 26.87	21.33	20.82	21.44	0.09	0.11	0.04	0.05

Continues in electronic form

TABLE 4
PHOTOMETRY COMPARISONS

Band	Δ mag	m_{lim}	N
<i>Internal – overlap regions</i>			
V	-0.003 ± 0.003	19.5	327
I	$+0.014 \pm 0.002$	19.0	357
B	-0.003 ± 0.004	19.5	160
<i>Wilson, Freedman & Madore (1990)</i>			
V	-0.041 ± 0.058	20.0	26
I	-0.032 ± 0.068	20.0	30
B	-0.024 ± 0.108	20.0	20
<i>Bersier et al. (2001)</i>			
V	-0.031 ± 0.047	18.5	39
B	-0.038 ± 0.033	18.5	31

TABLE 5
ARTIFICIAL STAR TESTS – RESULTS

Band	Mag.	Δ mag (meas-input)		
		median	mean	σ
V	15.5	-0.004	-0.007	0.019
	16.5	-0.009	-0.016	0.025
	17.5	-0.016	-0.026	0.040
	18.5	-0.028	-0.034	0.053
	19.5	-0.041	-0.052	0.092
	20.5	-0.062	-0.081	0.158
I	15.5	-0.014	-0.020	0.025
	16.5	-0.025	-0.032	0.040
	17.5	-0.039	-0.050	0.066
	18.5	-0.063	-0.076	0.084
	19.5	-0.076	-0.089	0.146
	20.5	-0.081	-0.128	0.248
B	16.5	-0.006	-0.012	0.021
	17.5	-0.013	-0.020	0.034
	18.5	-0.019	-0.030	0.048
	19.5	-0.029	-0.039	0.076
	20.5	-0.039	-0.055	0.132
	21.5	-0.046	-0.068	0.225